



Development of Design Analysis Methods for C/SiC Composite Structures

Roy M. Sullivan
Glenn Research Center, Cleveland, Ohio

Subodh K. Mital
University of Toledo, Toledo, Ohio

Pappu L.N. Murthy
Glenn Research Center, Cleveland, Ohio

Joseph L. Palko
Connecticut Reserve Technologies, Inc., Strongsville, Ohio

Jacques C. Cuneo and John R. Koenig
Southern Research Institute, Birmingham, Alabama

The NASA STI Program Office . . . in Profile

Since its founding, NASA has been dedicated to the advancement of aeronautics and space science. The NASA Scientific and Technical Information (STI) Program Office plays a key part in helping NASA maintain this important role.

The NASA STI Program Office is operated by Langley Research Center, the Lead Center for NASA's scientific and technical information. The NASA STI Program Office provides access to the NASA STI Database, the largest collection of aeronautical and space science STI in the world. The Program Office is also NASA's institutional mechanism for disseminating the results of its research and development activities. These results are published by NASA in the NASA STI Report Series, which includes the following report types:

- **TECHNICAL PUBLICATION.** Reports of completed research or a major significant phase of research that present the results of NASA programs and include extensive data or theoretical analysis. Includes compilations of significant scientific and technical data and information deemed to be of continuing reference value. NASA's counterpart of peer-reviewed formal professional papers but has less stringent limitations on manuscript length and extent of graphic presentations.
- **TECHNICAL MEMORANDUM.** Scientific and technical findings that are preliminary or of specialized interest, e.g., quick release reports, working papers, and bibliographies that contain minimal annotation. Does not contain extensive analysis.
- **CONTRACTOR REPORT.** Scientific and technical findings by NASA-sponsored contractors and grantees.

- **CONFERENCE PUBLICATION.** Collected papers from scientific and technical conferences, symposia, seminars, or other meetings sponsored or cosponsored by NASA.
- **SPECIAL PUBLICATION.** Scientific, technical, or historical information from NASA programs, projects, and missions, often concerned with subjects having substantial public interest.
- **TECHNICAL TRANSLATION.** English-language translations of foreign scientific and technical material pertinent to NASA's mission.

Specialized services that complement the STI Program Office's diverse offerings include creating custom thesauri, building customized databases, organizing and publishing research results . . . even providing videos.

For more information about the NASA STI Program Office, see the following:

- Access the NASA STI Program Home Page at <http://www.sti.nasa.gov>
- E-mail your question via the Internet to help@sti.nasa.gov
- Fax your question to the NASA Access Help Desk at 301-621-0134
- Telephone the NASA Access Help Desk at 301-621-0390
- Write to:
NASA Access Help Desk
NASA Center for AeroSpace Information
7121 Standard Drive
Hanover, MD 21076



Development of Design Analysis Methods for C/SiC Composite Structures

Roy M. Sullivan
Glenn Research Center, Cleveland, Ohio

Subodh K. Mital
University of Toledo, Toledo, Ohio

Pappu L.N. Murthy
Glenn Research Center, Cleveland, Ohio

Joseph L. Palko
Connecticut Reserve Technologies, Inc., Strongsville, Ohio

Jacques C. Cuneo and John R. Koenig
Southern Research Institute, Birmingham, Alabama

National Aeronautics and
Space Administration

Glenn Research Center

Acknowledgments

The authors are grateful for the funding through the CMC Design Methodology task under NASA's Next Generation Launch Technology (NGLT) Program.

Trade names or manufacturers' names are used in this report for identification only. This usage does not constitute an official endorsement, either expressed or implied, by the National Aeronautics and Space Administration.

Available from

NASA Center for Aerospace Information
7121 Standard Drive
Hanover, MD 21076

National Technical Information Service
5285 Port Royal Road
Springfield, VA 22100

Available electronically at <http://gltrs.grc.nasa.gov>

Development of Design Analysis Methods for C/SiC Composite Structures

Roy M. Sullivan

National Aeronautics and Space Administration

Glenn Research Center

Cleveland, Ohio 44135

Subodh K. Mital

The University of Toledo

Toledo, Ohio 43606

Pappu L.N. Murthy

National Aeronautics and Space Administration

Glenn Research Center

Cleveland, Ohio 44135

Joseph L. Palko

Connecticut Reserve Technologies, Inc.

Strongsville, Ohio 44136

Jacques C. Cuneo and John R. Koenig

Southern Research Institute

Birmingham, Alabama 35211

Summary

The stress-strain behavior at room temperature and at 1100 °C (2000 °F) was measured for two carbon-fiber-reinforced silicon carbide (C/SiC) composite materials: a two-dimensional plain-weave quasi-isotropic laminate and a three-dimensional angle-interlock woven composite. Micromechanics-based material models were developed for predicting the response properties of these two materials. The micromechanics-based material models were calibrated by correlating the predicted material property values with the measured values. Four-point beam bending subelement specimens were fabricated with these two fiber architectures, and four-point bending tests were performed at room temperature and at 1100 °C. Displacements and strains were measured at various locations along the beam and recorded as a function of load magnitude. The calibrated material models were used in concert with a nonlinear finite element solution to simulate the structural response of these two materials in the four-point beam bending tests. The structural response predicted by the nonlinear analysis method compares favorably with the measured response for both materials and for both test temperatures. Results show that the material models scale up fairly well from coupon to subcomponent level.

Introduction

Carbon-fiber-reinforced silicon carbide (C/SiC) composite technologies are being developed and advanced with the notion that C/SiC composites will find widespread use in the aerospace industry in the near future. Potential applications include turbine blades, combustion chambers, control surfaces, and thermal protection systems. Indeed, C/SiC composites are an attractive option for designers of advanced spacecraft and advanced space propulsion systems, since C/SiC composites are lightweight and since they maintain their strength and stiffness at high temperatures (ref. 1).

There are many challenges which must be overcome in order to advance C/SiC composite technologies to the point where the benefits of these composites are realized across a wide range of aerospace applications. For example, C/SiC composites are vulnerable to carbon fiber oxidation from environmental oxygen attack above 500 °C. Matrix microcracks formed during the fabrication process provide a free path for oxygen to attack the carbon fibers (refs. 2 to 4). Matrix cracking occurs because of the difference in the thermal expansion behavior between the carbon fiber and the SiC matrix in concert with temperature excursions resulting from processing. In addition, there may be a significant pore volume due to insufficient

infiltration of the matrix. Carbon fiber oxidation reduces the carbon fiber volume fraction over time, resulting in a loss of strength and stiffness.

Another obstacle is the fact that the material's stress-strain response is nonlinear even at low stress levels and that the material responds to stress differently in tension than in compression. These issues are not unrelated to the carbon oxidation issue. They all arise from the fact that the SiC matrix in C/SiC composites is usually severely cracked in the as-processed state. The preexisting matrix cracks will either close or extend upon loading, depending on the sign of the applied stress. In the compression mode, as cracks close, the material becomes stiffer, since a larger percentage of the SiC matrix volume will begin to carry load and resist compressive strain. In the tensile mode, as the applied loading is increased, matrix cracks continue to extend and matrix damage accumulation progresses to the point where the matrix effectively carries no load. At that point, applied stresses are resisted by only the fiber bundles. In addition, since the thermal expansion behavior is quite different between the carbon fibers and the SiC matrix, it is not surprising that the modulus and strength of C/SiC is significantly affected by the temperature. Temperature variations can cause variations in the mechanical interaction between the constituents as well as variations in the distribution of the constituent microstresses that develop from externally applied stresses. The nonlinear stress-strain response, the temperature-dependent properties, and the dissimilar response to tension and compression loading will all complicate the process of performing structural analyses of components made of C/SiC composites. In order for designers to utilize C/SiC in future spacecraft and propulsion designs, accurate structural analysis tools must be available that account for all of these factors.

In order to analyze three-dimensional C/SiC composite structures with numerical approaches such as the finite element method, engineering constants for the three principal material directions are required and these must be defined as a function of stress and temperature. Recently, experimental studies have been conducted to obtain the tension and compression stress-strain behavior of two C/SiC composites: a two-dimensional plain-weave quasi-isotropic laminate and a three-dimensional angle-interlock woven composite. The in-plane principal material direction stress-strain response for both materials was measured as a function of temperature (ref. 5).

Material characterization efforts based solely on testing can be quite expensive. In addition, some properties can be quite difficult to obtain experimentally, such as the out-of-plane tension stiffness. For these purposes, material modeling efforts can be quite useful in supplementing experimental material characterization efforts. Micromechanics-based analysis methods have been developed to predict the response properties of plain weave ceramic matrix composites (refs. 6 and 7). The methodology employed was based on composite micromechanics in combination with the classical laminate theory.

Specifically, the micromechanics approach was used to predict the properties of each individual lamina of the two-dimensional laminate. The properties obtained for each lamina were then used along with the classical lamination theory to obtain the overall homogenized properties of the C/SiC composite. The resulting equations were programmed into a computer code known as W-CEMCAN (ref. 8).

This report presents recent analytical, numerical and experimental efforts conducted to develop accurate structural analysis methods for C/SiC composite structures. The stress-strain response that was measured in the tension and compression testing is discussed, and the average tangent modulus in the principal material directions was obtained as a function of the composite stress value. Also, micromechanics-based material models are exercised, and the predicted composite stiffness is correlated with the measured tangent moduli. The correlation is performed at various stress levels and at two temperatures to obtain an effective matrix modulus as a function of composite stress and temperature for the two- and three-dimensional materials. Using the effective matrix modulus, W-CEMCAN can be used to predict the full set of engineering constants for the two composite materials as a function of stress and temperature. From the engineering constants, the elements of the elastic stiffness tensor are calculated for each material as a function of stress and temperature.

This report also presents results from four-point beam bending tests that were conducted on beam specimens fabricated with the two-dimensional and three-dimensional composite materials. Strains and displacements at the midspan of the beam were measured and recorded as a function of the load magnitude. A nonlinear structural analysis of the four point beam specimen was performed using ABAQUS (ref. 9), a user-supplied subroutine and the elastic stiffness tensor calculated by W-CEMCAN. Strains and displacements at the midspan were predicted, and these were compared to the measured strains and displacements to judge the accuracy of the analysis approach. The modeling and testing reported here are restricted to an inert environment. Therefore, oxidation related issues are not addressed.

Material Modeling

A micromechanics-based computer code such as W-CEMCAN takes as input the weave architecture, constituent material volume fraction, void volume fraction, and constituent thermal and mechanical properties. The philosophy adopted here is that the carbon fiber and pyrocarbon coating properties are fairly well quantified but that the matrix in situ modulus is not known. The properties of the SiC matrix can not be measured separately, since the state of the SiC matrix in the composite system is not the same as the state of silicon carbide in bulk form. Since the in situ matrix modulus is not known, it is necessary to determine the modulus as a function of

temperature and composite stress by exercising the micromechanics tool and by comparing the predicted composite properties with the measured properties. In this manner, a calibrated effective matrix modulus is obtained through a trial-and-error approach as a function of temperature and stress. Once this is achieved, a full set of three-dimensional composite properties over a range of temperatures and stresses can be predicted and used in the finite element analyses. Since the coupon-level composite material testing and the subelement testing was done at room temperature and at an elevated temperature of 1100 °C (2000 °F), the composite properties were predicted using the micromechanics approach at these two temperatures.

The two materials of interest in this study are (1) a two-dimensional quasi-isotropic balanced weave composite and (2) a three-dimensional angle-interlock woven composite. Both materials were fabricated using T-300 carbon fibers with pyrocarbon coating and were infiltrated with a SiC matrix via chemical vapor infiltration (CVI). Both materials were manufactured by GE Power Systems Composites of Newark, DE, and contain a total fiber volume fraction of approximately 40 percent.

Two-Dimensional Balanced Weave Quasi-Isotropic Laminate

The two-dimensional quasi-isotropic laminate was fabricated using a plain weave fabric with the ply layup [0/45/90/-45]_{2s}. The fabric was woven using 1k tows (1000 filaments per tow). The fiber architecture for the two-dimensional laminate is illustrated by the sketch and photomicrograph shown in figure 1. Also, the principal material coordinates (*w*, *f*, *n*) are identified in the sketch, where *w* is the warp direction, *f* is the fill direction, and *n* is the direction normal to those.

The typical stress-strain response for the two-dimensional quasi-isotropic material measured in the warp direction during multiple load-unload tests are shown in figures 2 and 3. Figure 2 shows a typical warp direction tensile stress-strain response at room temperature and at 1100 °C, and figure 3 shows a typical warp direction compression response at these temperatures. The fill direction exhibits a similar stress-strain response in both tension and compression.

Although the compression response is only slightly nonlinear, the nonlinear tension response is more pronounced. In order to input the nonlinear stress-strain behavior into a structural analysis solution, the variation of the tangent modulus with stress level must be quantified. The tangent modulus at the specific stress magnitudes of 0, 34.5, 69, 138, and 276 MPa (0, 5, 10, 20, and 40 ksi) was determined graphically for all stress-strain curves. The tangent modulus at these specific stress magnitudes was then averaged for each set of test conditions (material direction and test temperature). This yields an average tension and compression tangent modulus as a function of stress level for the two material directions and

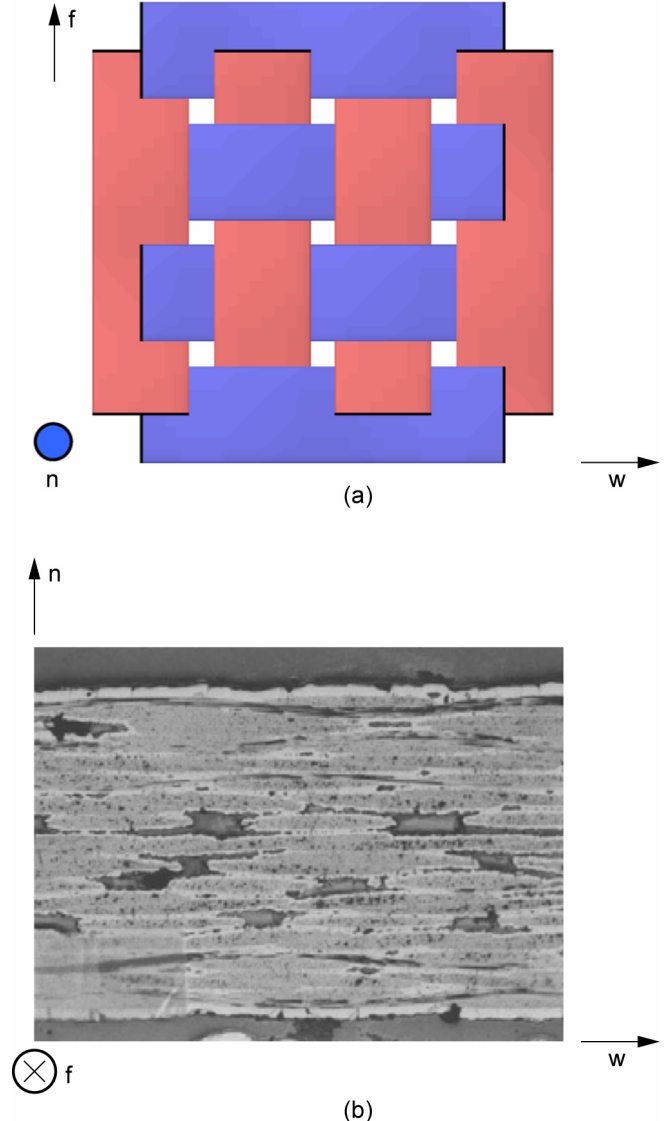


Figure 1.—Two-dimensional quasi-isotropic C/SiC laminate, where *w* is warp direction, *f* is fill direction, and *n* is the direction normal to those. (a) Plain weave ply. (b) Optical microscopy image of balanced weave.

the two test temperatures. These variations are shown in figures 4 and 5. Figure 4 shows the average tension and compression tangent modulus for the warp and fill directions as a function of stress level at room temperature, while figure 5 shows this at 1100 °C.

For both temperatures and material directions, the tension modulus decreases with increasing stress level. It may be argued that the warp and fill compression moduli at room temperature remain fairly constant with stress level, since neither modulus varies more than 15 GPa (2 Ms) over the

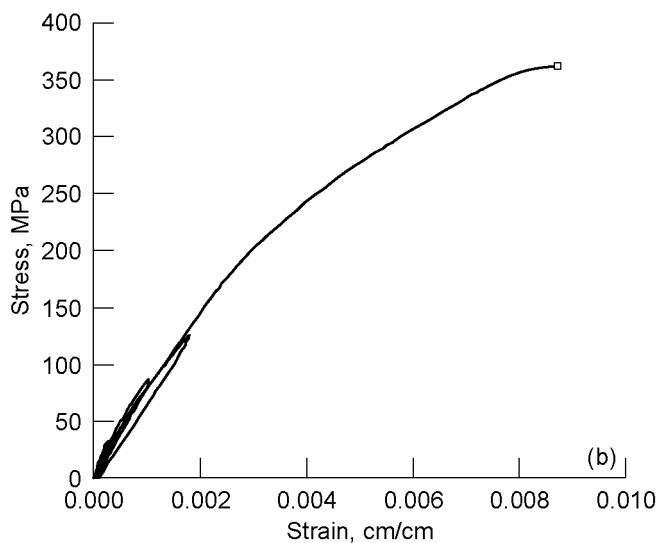
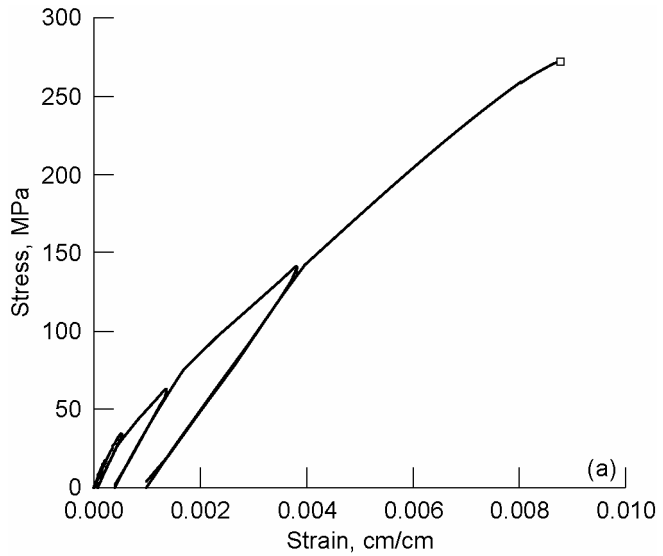


Figure 2.—Typical warp tensile stress-strain response of two-dimensional quasi-isotropic C/SiC laminate measured with a multiple load-unload tensile test. (a) Room temperature. (b) 1100 °C.

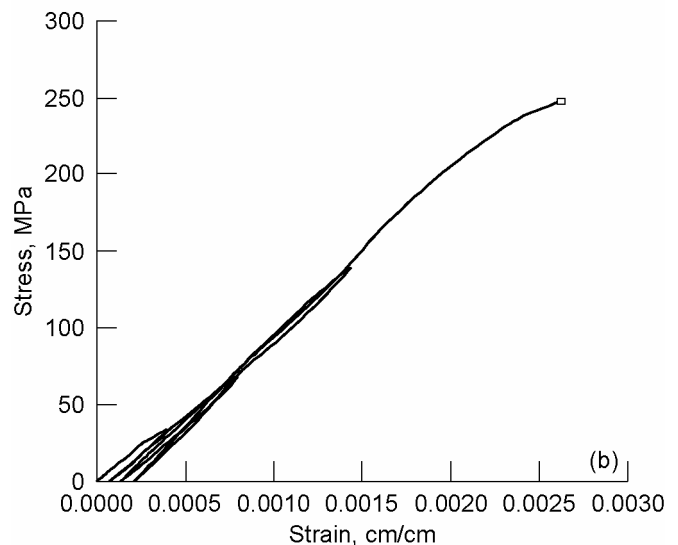
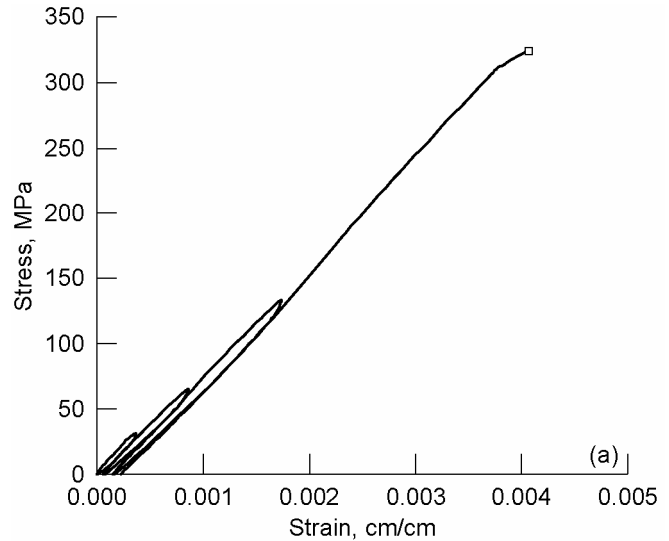


Figure 3.—Typical warp compression stress-strain response of two-dimensional quasi-isotropic C/SiC laminate measured with multiple load-unload compression test. (a) Room temperature. (b) 1100 °C.

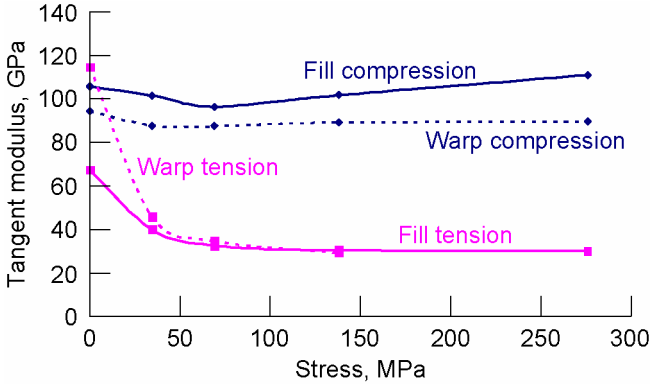


Figure 4.—Average measured tension and compression tangent moduli at room temperature for warp and fill directions versus stress level for two-dimensional balanced weave quasi-isotropic C/SiC laminate.

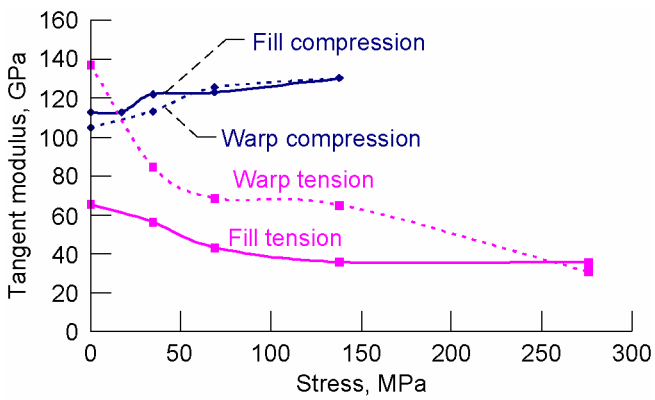


Figure 5.—Average measured tension and compression tangent modulus at 1100 °C for warp and fill directions versus stress level for two-dimensional balanced weave quasi-isotropic C/SiC laminate.

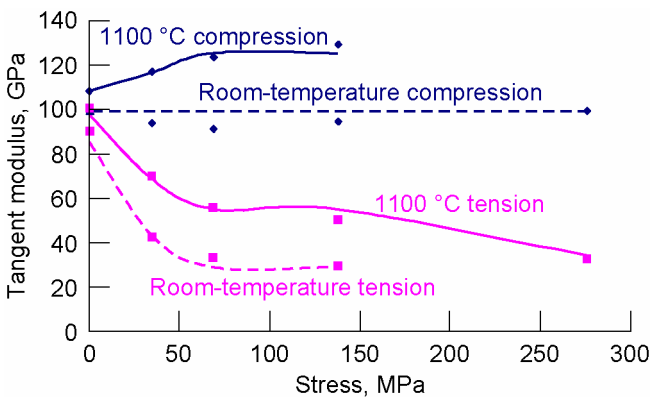


Figure 6.—Comparison of measured (points) and W-CEMCAN-predicted (lines) in-plane tension and compression tangent modulus versus stress level for two-dimensional balanced weave quasi-isotropic C/SiC laminate at room temperature and 1100 °C.

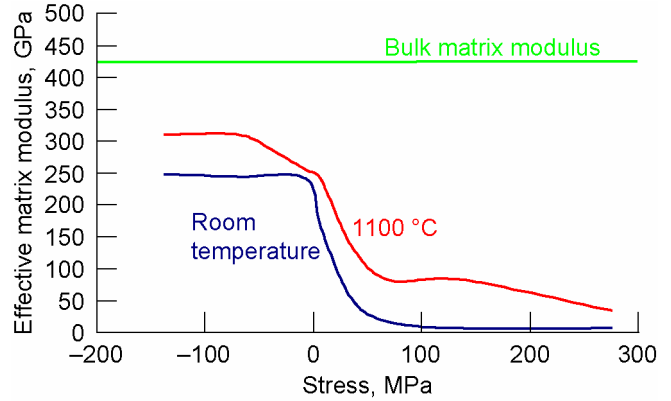


Figure 7.—Calibrated effective matrix modulus versus applied composite stress for two-dimensional balanced weave quasi-isotropic C/SiC laminate at room temperature and at 1100 °C.

entire stress range. The warp and fill compression moduli at 1100 °C, however, vary by about 25 GPa (5 Msi) over the same stress range and exhibit a definite increase with increasing stress.

One would expect the measured warp stiffness and fill stiffness to be equal because of the [0/45/90/-45]_{2S} layup and since the laminates were constructed with a balanced plain weave fabric. However, it is obvious in figures 4 and 5 that although their variation with stress is similar, the warp and fill tangent moduli are not identical at all stress values. It is likely that the small number of test replicas performed to obtain the average moduli resulted in the differences observed in the average warp and fill moduli. Because a balanced weave architecture is input into W-CEMCAN, the micromechanics approach would not be capable of predicting an unbalanced material behavior. As a result, for the purposes of our structural analysis solution, it will be assumed that the warp and fill moduli are equal.

To this end, the warp and fill stiffness at each stress level were averaged and an average in-plane modulus as a function of stress level was obtained for the compression and tension responses at the two temperatures. In figure 6, the average in-plane modulus is plotted for different stress levels at both room temperature and 1100 °C. Both experimental values and those predicted with W-CEMCAN are shown. The close agreement between the measured and predicted in-plane moduli was obtained through a trial-and-error approach by continuously varying the SiC matrix modulus input to the W-CEMCAN solution. By matching the measured and predicted composite moduli at the various stress magnitudes and at both temperatures, an effective matrix modulus can be deduced for each stress and temperature condition. This variation is shown in figure 7. It is interesting to note that the effective matrix modulus is significantly less than the modulus of fully-dense silicon carbide

TABLE I.—PREDICTION OF TWO-DIMENSIONAL BALANCED WEAVE QUASI-ISOTROPIC C/SiC LAMINATE PROPERTIES AT ROOM TEMPERATURE

Stress state		Property ^a				
		Young's modulus, GPa (Msi)		Shear modulus, GPa (Msi)		
		$E_w = E_f$	E_n	G_{wf}	G_{wn}	
Tensile	Stress = 0 Matrix Young's modulus, $E_m = 165$ GPa (24 Msi)	77.91 (11.30)	40.33 (5.85)	31.72 (4.60)	22.48 (3.26)	0.20
	Stress > 69 MPa (10 ksi) Matrix Young's modulus, $E_m = 6.9$ GPa (1 Msi)	28.96 (4.20)	8.55 (1.24)	10.34 (1.50)	4.34 (0.63)	0.22
Compressive	Matrix Young's modulus, $E_m = 241$ GPa (35 Msi)	100.66 (14.60)	56.54 (8.20)	39.51 (5.73)	32.68 (4.74)	0.27

^aSubscripts w , f , and n indicate warp, fill, and normal directions, respectively (see fig. 1).

TABLE II.—PREDICTION OF TWO-DIMENSIONAL BALANCED WEAVE QUASI-ISOTROPIC C/SiC LAMINATE PROPERTIES AT 1100 °C (2000 °F)

Stress state		Property ^a				
		Young's modulus, GPa (Msi)		Shear modulus, GPa (Msi)		
		$E_w = E_f$	E_n	G_{wf}	G_{wn}	
Tensile	Stress = 0 Matrix Young's modulus, $E_m = 241$ GPa (35 Msi)	100.66 (14.60)	56.54 (8.20)	39.51 (5.73)	32.68 (4.74)	0.27
	Stress > 103 MPa (15 ksi) Matrix Young's modulus, $E_m = 55$ GPa (8 Msi)	46.20 (6.70)	19.31 (2.80)	16.55 (2.40)	10.34 (1.50)	0.27
	Stress > 241 MPa (35 ksi) Matrix Young's modulus, $E_m = 6.9$ GPa (1 Msi)	28.96 (4.20)	8.96 (1.30)	10.34 (1.50)	4.34 (0.63)	0.20
Compressive	Stress = 0 Matrix Young's modulus, $E_m = 241$ GPa (35 Msi)	100.66 (14.60)	56.54 (8.20)	39.51 (5.73)	32.68 (4.74)	0.27
	Stress > 69 MPa (10 ksi) Matrix Young's modulus, $E_m = 310$ GPa (45 Msi)	125.48 (18.20)	77.91 (11.30)	59.29 (8.60)	53.78 (7.80)	0.28

^aSubscripts w , f , and n indicate warp, fill, and normal directions, respectively (see fig. 1).

in bulk form, which is approximately 420 GPa (61 Msi) (ref. 10). This is not surprising because the matrix contains numerous cracks and significant pore volumes in the as-fabricated C/SiC composite. This difference is most pronounced in the tension regime.

It should also be noted that the effective matrix modulus is lower for room temperature than for 1100 °C at all composite stress values. This is expected since 1100 °C is in the vicinity

of the processing temperature, the temperature at which the residual stresses in the matrix should be at a minimum.

Finally, using the variation of the calibrated effective matrix modulus with stress level shown in figure 7 and utilizing W-CEMCAN, the engineering constants were computed as a function of composite stress for the two-dimensional quasi-isotropic material both at room temperature and 1100 °C. These are summarized in tables I and II, respectively.

Three-Dimensional Angle-Interlock Woven Composite

The fiber architecture for the three-dimensional angle-interlock woven composite along with its microstructure in two planar directions, is shown in figure 8. The three-dimensional woven composite used 3k tows (3000 filaments per tow). The warp tows are woven, in an up and down pattern, through an array of pick (fill) tows. The principal material coordinates for the composite are designated as (w' , f , n): the w' -direction is the “warp” direction (not a true warp direction, as the warp weavers make an angle of approximately 10° with the w' -direction), the f -direction is the fill direction, and the n -direction is the direction normal to those. The orientation of the (w' , f , n) coordinate axes with respect to the weave architecture is shown in figure 8. The axial length that is required for a warp weaver to complete one up-and-down cycle is 2.857 cm (1.125 in.). Simple calculations done on the microstructure show that approximately 70 percent of the total fibers are in the warp direction.

Typical w' -direction tensile stress-strain curves are shown in figure 9. Figure 9(a) shows a typical room temperature response, and figure 9(b) shows a typical response at 1100 °C. Figure 10 shows typical w' -direction compression stress-strain curves for room temperature and 1100 °C. The fill tensile and fill compression stress-strain responses exhibit a similar behavior as that of the w' -direction at both temperatures, although the fill stiffness is significantly less than the w' -direction because of the difference in carbon fiber volume fractions in the two directions.

Again the tangent modulus for each stress-strain curve was determined graphically at 0, 34.5, 69, 138, and 276 MPa (0, 5, 10, 20, and 40 ksi). The tangent moduli at each stress level were averaged, and the average tangent modulus for each test condition (material direction and temperature) was determined as a function of stress level. The variation of the average tangent modulus with stress is shown in figures 11 and 12. Figure 11 shows the average tangent modulus versus stress level at room temperature, and figure 12 shows the average tangent modulus at 1100 °C. It is interesting to note that in the tension mode the w' -direction stiffness is approximately twice that of the f -direction for all stress levels and for both temperatures. This is consistent with the fiber volume fraction in the two material directions. Remember that 70 percent of the total carbon fiber volume fraction is oriented in the w' -direction and 30 percent is oriented in the f -direction. The same can be said about the w' -direction and f -direction moduli in the compression mode at 1100 °C. The w' -direction compression modulus at room temperature, however, is not twice the value of the fill-direction modulus.

The measured and predicted w' - and f -direction moduli at different stress levels are shown in figures 13 and 14 for room temperature and 1100 °C, respectively. Again the predicted moduli are obtained through a trial and error procedure by varying the matrix modulus. This yields a calibrated effective matrix modulus as a function of stress level. The calibrated effective matrix modulus is plotted in figure 15 for both temperatures. Again, the calibrated matrix modulus is significantly less than the modulus of SiC in bulk form.

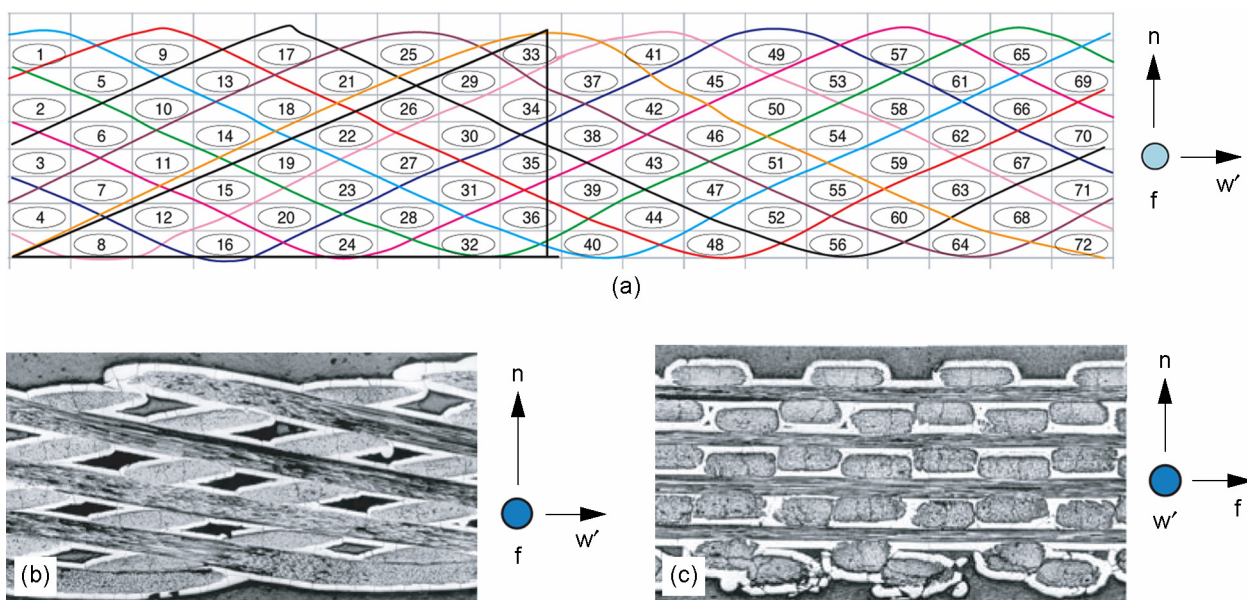


Figure 8.—Three-dimensional angle-interlock woven C/SiC composite, where f is direction of fill tows. (a) Sketch of fiber architecture. (b) Optical microscopy image (50 \times) of fill ends. (c) Optical microscopy image (50 \times) of warp ends.

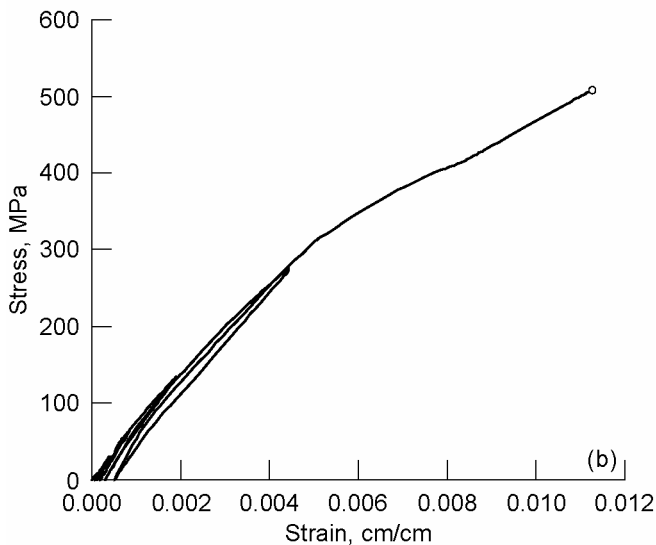
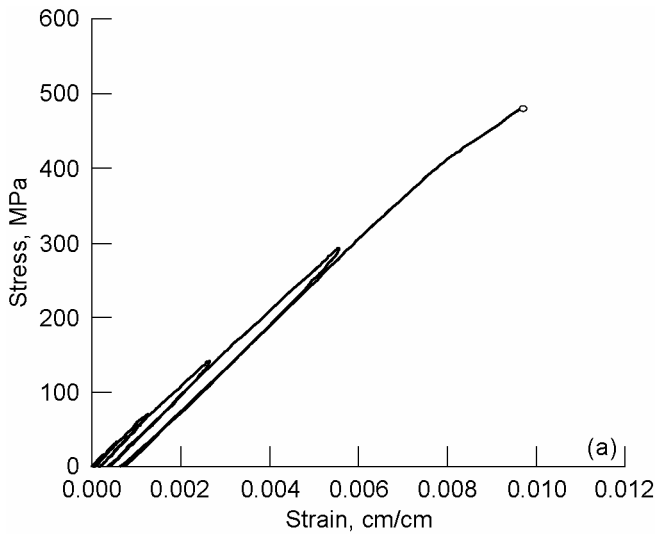


Figure 9.—Typical w'-direction tensile stress-strain curve of three-dimensional angle-interlock woven C/SiC composite measured with multiple load-unload tensile test. (a) Room temperature. (b) 1100 °C.

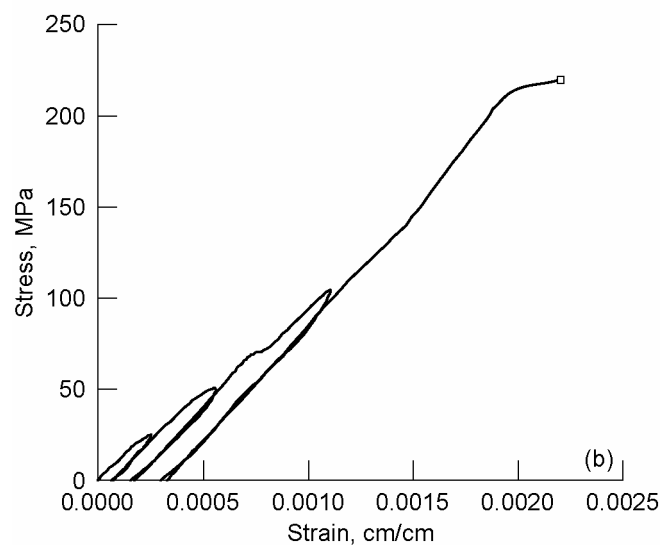
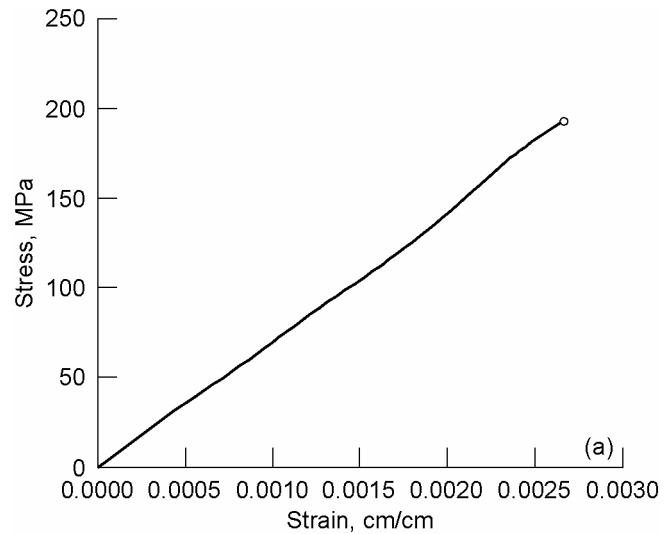


Figure 10.—Typical w'-direction compression stress-strain curve of three-dimensional angle-interlock woven C/SiC composite measured with multiple load-unload compression test. (a) Room temperature. (b) 1100 °C.

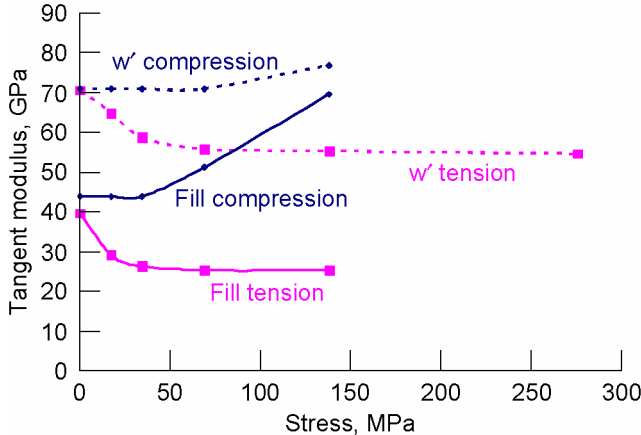


Figure 11.—Average tangent modulus versus stress level for three-dimensional angle-interlock woven C/SiC composite at room temperature.

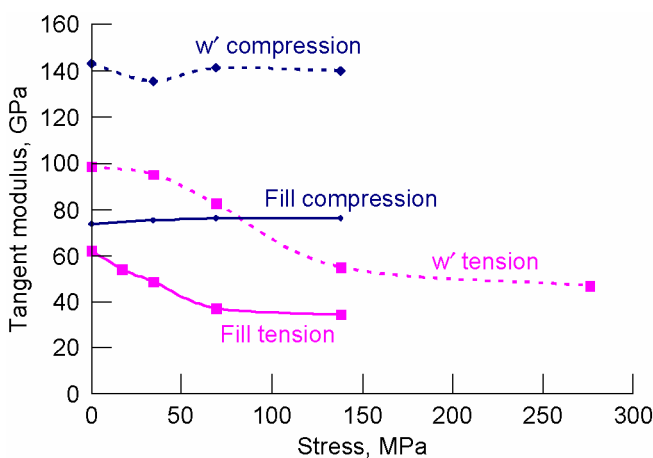


Figure 12.—Average tangent modulus versus stress level for three-dimensional angle-interlock woven C/SiC composite at 1100 °C.

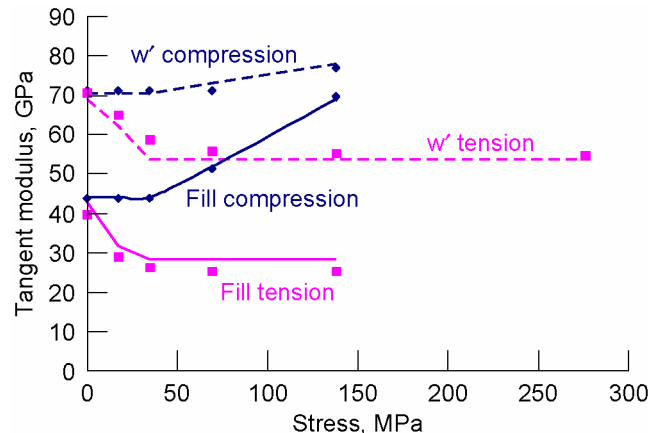


Figure 13.—Comparison of measured (points) and W-CEMCAN-predicted (lines) tangent modulus versus stress level for three-dimensional angle-interlock woven C/SiC composite at room temperature.

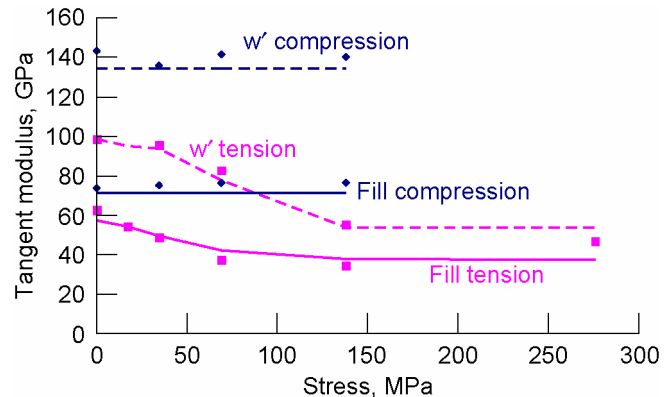


Figure 14.—Comparison of measured (points) and W-CEMCAN-predicted (lines) tangent modulus versus stress level for three-dimensional angle-interlock woven C/SiC composite at 1100 °C.

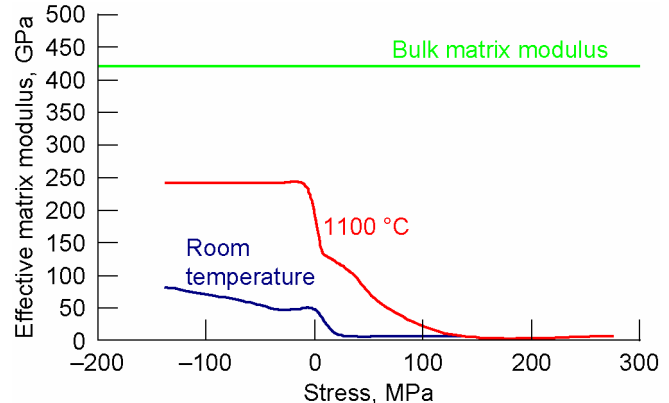


Figure 15.—Calibrated effective matrix modulus versus applied stress for three-dimensional angle-interlock woven C/SiC composite at room temperature and 1100 °C.

TABLE III.—PREDICTION OF THREE-DIMENSIONAL ANGLE-INTERLOCK WOVEN C/SiC COMPOSITE PROPERTIES AT ROOM TEMPERATURE

Stress state		Property ^a					
		Young's modulus, GPa (Msi)			Shear modulus, GPa (Msi)		
		$E_{w'}$	E_f	E_n	$G_{w'f}$	$G_{w'n}$	
Tensile	Stress = 0 Matrix Young's modulus, $E_m = 48.3$ GPa (7 Msi)	73.08 (10.60)	44.82 (6.50)	22.75 (3.30)	11.03 (1.60)	11.03 (1.60)	0.11
	Stress > 34.5 MPa (5 ksi) Matrix Young's modulus, $E_m = 10.3$ GPa (1.5 Msi)	59.29 (8.60)	31.72 (4.60)	9.65 (1.40)	4.48 (0.65)	4.48 (0.65)	0.10
	Stress > 69 MPa (10 ksi) Matrix Young's modulus, $E_m = 6.9$ GPa (1 Msi)	57.23 (8.30)	29.65 (4.30)	7.58 (1.10)	3.45 (0.50)	3.45 (0.50)	0.10
Compressive	Stress > 69 MPa (10 ksi) Matrix Young's modulus, $E_m = 58.6$ GPa (8.5 Msi)	75.84 (11.00)	47.57 (6.90)	24.82 (3.60)	12.41 (1.80)	12.41 (1.80)	0.11
	Stress > 103 MPa (15 ksi) Matrix Young's modulus, $E_m = 103$ GPa (15 Msi)	89.63 (13.00)	58.61 (8.50)	33.78 (4.90)	16.55 (2.40)	16.55 (2.40)	0.12

^aSubscripts w' , f , and n indicate principle material directions (see fig. 8).

TABLE IV.—PREDICTION OF THREE-DIMENSIONAL ANGLE-INTERLOCK WOVEN C/SiC COMPOSITE PROPERTIES AT 1100 °C (2000 °F)

Stress state		Property ^a					
		Young's modulus, GPa (Msi)			Shear modulus, GPa (Msi)		
		$E_{w'}$	E_f	E_n	$G_{w'f}$	$G_{w'n}$	
Tensile	Stress = 0 Matrix Young's modulus, $E_m = 138$ GPa (20 Msi)	102.04 (14.80)	70.33 (10.20)	45.51 (6.60)	23.44 (3.40)	23.44 (3.40)	0.13
	Stress > 34.5 MPa (5 ksi) Matrix Young's modulus, $E_m = 90$ GPa (13 Msi)	87.56 (12.70)	58.61 (8.50)	35.85 (5.20)	18.62 (2.70)	18.62 (2.70)	0.13
	Stress > 69 MPa (10 ksi) Matrix Young's modulus, $E_m = 48$ GPa (7 Msi)	74.46 (10.80)	47.57 (6.90)	26.20 (3.80)	13.44 (1.95)	13.44 (1.95)	0.12
Compressive	Matrix Young's modulus, $E_m = 241$ GPa (35 Msi)	132.38 (19.20)	94.46 (13.70)	64.12 (9.30)	31.72 (4.60)	31.72 (4.60)	0.13

^aSubscripts w' , f , and n indicate principle material directions (see fig. 8).

Furthermore, it should be noted that while comparing figures 7 and 15 it is apparent that the effective matrix modulus is lower for the three-dimensional woven composite than for the two-dimensional composite. This is likely the result of less matrix infiltration in the three-dimensional composite, resulting in a higher void volume and lower matrix volume.

Finally, using W-CEMCAN and the effective matrix modulus shown in figure 15, the engineering constants were computed as a function of composite stress for the three-dimensional angle-interlock woven material both at room temperature and 1100 °C. These are summarized in tables III and IV, respectively.

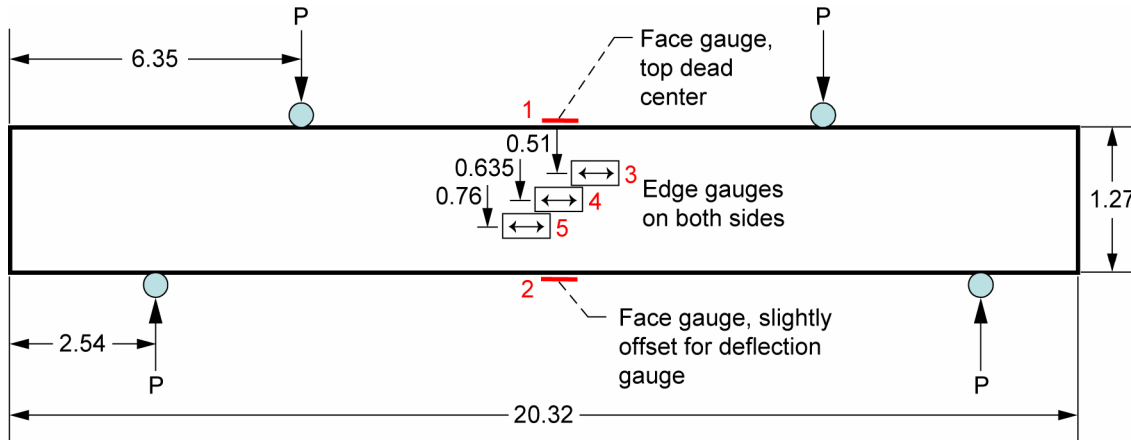


Figure 16.—Four-point flexure subelement showing loading and strain gauge locations. All values are in centimeters.

Subelement Test: Four-Point Flexure Specimen

Four-point beam bending tests were performed with both the two-dimensional laminate and three-dimensional woven C/SiC composite materials. Tests were conducted at both room temperature and 1100 °C. The four-point beam bending test configuration is illustrated in figure 16. Beam bending specimens were fabricated 20.32 cm (8.0 in.) long, 1.27 cm (0.5 in.) deep, and 0.216 cm (0.085 in.) thick. The two-dimensional laminate specimens were fabricated such that the plane of loading and bending was coincident with the fabric (lamina) planes. The three-dimensional woven angle interlock beam bending specimens were fabricated such that the beam axial direction is coincident with the f-direction and the beam depth direction is coincident with the w'-direction.

The four-point beam bending specimens were simply supported, with supports located 2.54 cm (1.0 in.) from the end of the beam. Two concentrated loads were applied 6.35 cm (2.5 in.) from both ends of the beam. A deflection gauge was mounted at the midspan, on the bottom face of the beam. Eight strain gauges were mounted to the beam at five spatial locations. The five locations are identified in figure 16. One strain gauge was located at the top face of the beam (strain gauge location 1) and a second gauge was located on the bottom face (location 2). Two strain gauges (one on each side of the beam) were located at location 3. Location 3 was at approximately the midspan of the beam, at a depth of 0.51 cm (0.2 in.) from the top. Two gauges (one on each side of the beam) were located at location 4 and at location 5. Location 4 was at the midspan of the beam at a depth of 0.635 cm (0.25 in.) from the top. Location 5 was at approximately the midspan of the beam at a depth of 0.76 cm (0.3 in.) from the top. The strain gauges at locations 1 through 5 all measured the strain in the axial direction.

Finite Element Analysis of Four-Point Flexure Specimen

Approach

In order to predict the structural response of the C/SiC four-point beam bending specimens, a combination of analysis tools were utilized. These include the nonlinear structural solution routine in ABAQUS (ref. 9), the W-CEMCAN micromechanics tool, and a user-defined material subroutine (UMAT). The W-CEMCAN micromechanics tool predicts the elastic stiffness tensor as a function of temperature and composite stress magnitude, using the carbon fiber and pyro-carbon coating properties along with the calibrated effective matrix modulus shown in figures 7 and 15. The UMAT was written to supply the stress-dependent stiffness tensor to the nonlinear ABAQUS solution. The UMAT is listed in the appendix.

At the start of each load step, material property values for each finite element are input as a function of temperature and the composite stress state. The solution of the finite element equations is performed using ABAQUS, and the material property values are updated by the UMAT based upon the current stress predictions. The ABAQUS solution is repeated with the updated properties. This process is repeated until convergence is achieved. Once convergence (equilibrium) is achieved the next load increment is added and the process is repeated for the next load step.

The four-point flexure specimen was modeled using a total of 10 920 nodes and 5120 elements. The ABAQUS C3D8 element, an eight-node linear brick element, was used throughout the model. Four layers of elements of equal thickness were used through the thickness of the beam.

Results

Figure 17 shows the load versus midspan displacement measured in the four-point beam bending experiment for the two-dimensional quasi-isotropic material tested at room temperature. Figure 17 also contains the numerical results from two finite element solutions: a linear analysis and a nonlinear analysis that utilizes the UMAT. The linear analysis used a constant warp and fill material moduli, which was the initial

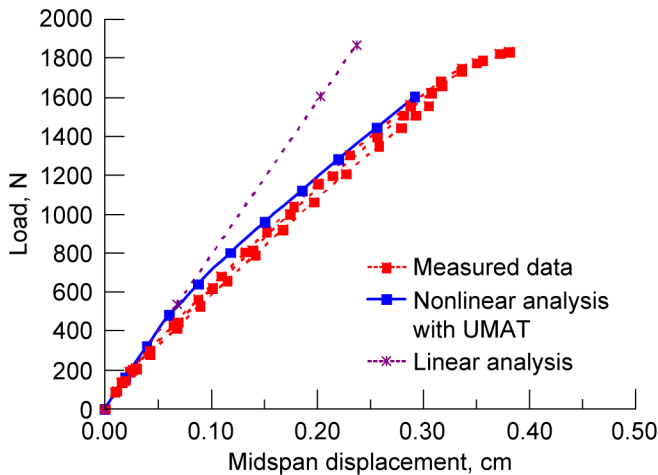


Figure 17.—Comparison of measured and predicted load versus midspan displacement of two-dimensional quasi-isotropic C/SiC laminate four-point flexure specimen at room temperature. UMAT is user-defined material subroutine.

moduli measured at zero stress. As expected, the displacements predicted with the linear model are in good agreement with the measured values at low load levels, but deviate from the measured response at higher load levels. The nonlinear load-displacement curve was obtained using a nonlinear analysis solution in ABAQUS and the user-defined subroutine. The nonlinear solution routine appears to provide a good correlation with the measured load-displacement response. The nonlinear load-displacement curve is due to the fact that as the loading is increased, tension stresses become elevated, and the material on the tension side of the neutral axis begins to soften or becomes more compliant, as evidenced by figures 3 and 4.

Figure 18 shows the comparison between the measured and predicted axial strains at gauge locations 2, 3, and 5. The strains at these three locations are plotted versus loading magnitude. Now since the tangent tensile modulus decreases with increasing stress and since the tangent compressive modulus remains constant with increasing stress, when the applied loads are increased a larger percentage of the beam depth must be on the tensile side of the neutral axis in order to maintain force equilibrium. As a result, the neutral axis moves to a higher depth of the beam. This is evident in figure 18 where it is observed that the axial strain measured by the gauge at location 3 is initially compressive, but as the applied load is increased, the gauge reads a positive strain, indicating that the neutral axis is shifted up and crosses over the location 3 depth. It is evident in figure 18 that the numerical solution mimics the strain reversal in the gauge response and that the strain predictions are in good agreement with the measured response.

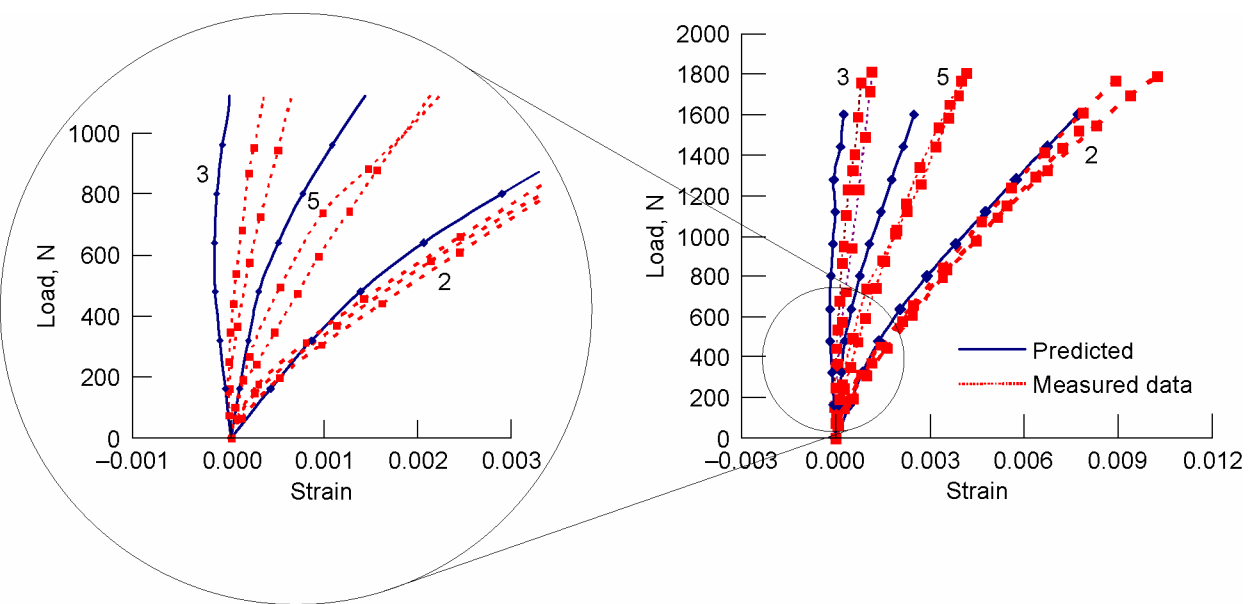


Figure 18.—Comparison of measured and predicted load versus strain at gauge locations 2, 3, and 5 (see fig. 16) for two-dimensional quasi-isotropic C/SiC laminate four-point flexure specimen at room temperature.

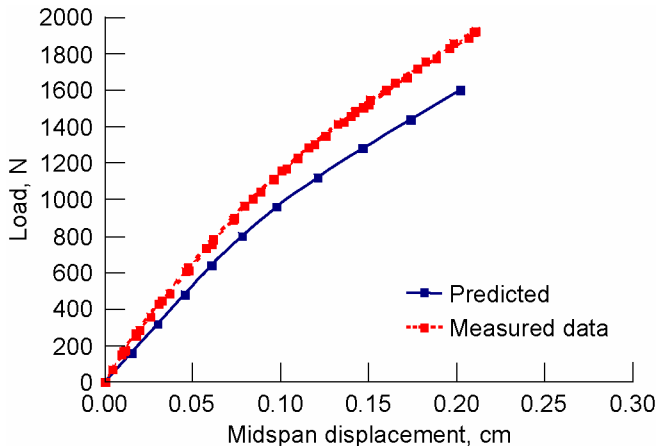


Figure 19.—Comparison of measured and predicted load versus midspan displacement of two-dimensional quasi-isotropic C/SiC laminate four-point flexure specimen at 1100 °C.

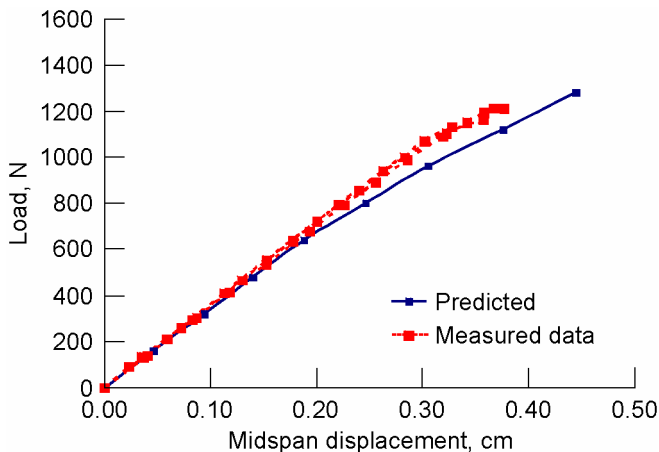


Figure 20.—Comparison of measured and predicted load versus midspan displacement for three-dimensional angle-interlock woven C/SiC four-point flexure specimen at room temperature.

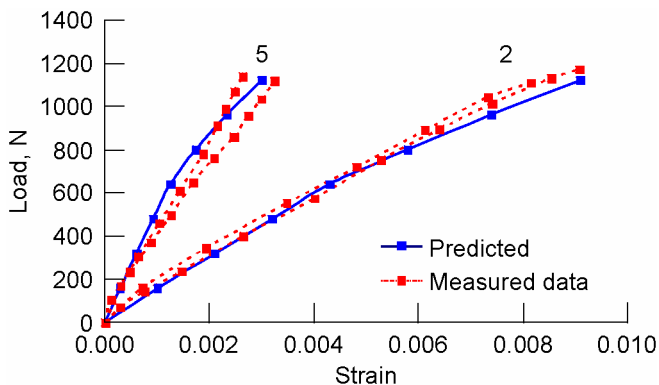


Figure 21.—Comparison of measured and predicted load versus strain at gauge locations 2 and 5 for three-dimensional angle-interlock woven C/SiC four-point flexure specimen at room temperature.

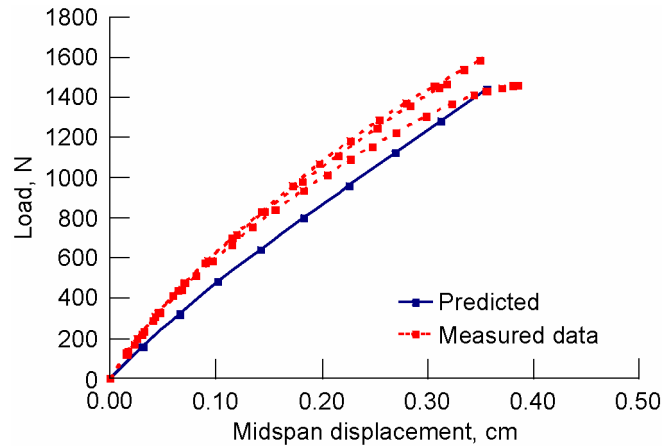


Figure 22.—Comparison of measured and predicted load versus midspan displacement for three-dimensional angle-interlock woven C/SiC four-point flexure specimen at 1100 °C.

Figure 19 shows the load versus midspan displacement curve for the two-dimensional quasi-isotropic material at 1100 °C. Again, the predicted load-displacement response obtained using the nonlinear solution routine is in good agreement with the measured response. Unfortunately, it was not possible to measure the strain response because of the inability to adhere strain gauges on the specimen at 1100 °C. As such, there were no strain measurements made during the 1100 °C tests and no strain comparisons between the measured and predicted strain responses could be made.

Figure 20 is a comparison of the measured and predicted load versus midspan displacement curve for the three-dimensional angle-interlock woven composite specimen tested at room temperature. Figure 21 is a comparison of the measured and predicted strains at gauge locations 2 and 5. The predicted load-displacement and the load versus strain predictions are in good agreement with the measured responses. In addition, the measured results are consistent and repeatable for all conditions.

A comparison of the measured and predicted load versus midspan displacement is shown in figure 22 for the three-dimensional angle-interlock woven test specimen tested at 1100 °C. Again, the predicted results compare reasonably well with the measured load-displacement response.

Concluding Remarks

Due to the effect of processing-induced residual stresses on the silicon carbide matrix, the measured stress-strain behavior in C/SiC composites is nonlinear and temperature dependent. As such, the tangent modulus is a function of temperature and the applied stress value. A calibrated effective matrix modulus was defined as a function of stress and temperature by exercising previously developed micromechanics-based material models and comparing the model predictions with the

measured stiffness values. The calibrated matrix modulus was determined as a function of composite stress magnitude for two temperatures and two fiber architectures. The effective matrix stiffness was found to be only a fraction of the bulk silicon carbide stiffness reported in the literature. Using the effective matrix modulus, the engineering constants were computed using W-CEMCAN. The computed material properties were then used to predict the nonlinear structural response of a four-point flexure specimen to see how the material models scale up to subelement level analyses. Results show that, in general, the comparison between the predicted and measured displacements and strains is reasonable for both two- and three-dimensional composite systems.

The four-point bending test was chosen as the subelement test problem because of its simplicity. As such, the user subroutine used for this solution need not be very sophisticated.

Future work should include extending the analysis method to problems that are progressively more complicated in order to continue the development of robust and computationally efficient algorithms for updating the elastic stiffness tensor.

The tension and compression specimen tests and the four-point bending tests reported here were conducted in an inert environment. The analysis methods employed did not address oxidation of the carbon constituents. Future work should involve extensive mechanical testing in air and other oxidative environments and the development of analysis methods that include the effects of oxidation on the material stiffness and strength.

Glenn Research Center
National Aeronautics and Space Administration
Cleveland, Ohio, February 2006

Appendix—UMAT Subroutine

Following is a listing of the user-defined material subroutine (UMAT) used with the ABAQUS finite element analysis.

```
c
c Orthotropic Material Properties User Mat Subroutine
c
SUBROUTINE UMAT(Stress, statev, ddsdde,sse,spd,scd,rpl,ddsddt,
1 Drplde, Drpldt,Stran,Dstran,time,dtime,Temp,Dtemp,predef,Dpred,
2 CMNAME, NDi, Nshr, Ntens, Nstatv, Props, Nprops, Coords, Drot,
3 Pnewdt, Celent, Dfgrd0,Dfgrd1,Noel, Npt, layer,Kspt, Kinc)

Include 'Aba_param.inc'
Character*8 CMNAME
c23456789012345678901234567890123456789012345678901234567890
Dimension Stress(Ntens),Statev(Nstatv),DDSDDE(Ntens,Ntens),
1 Ddsddt(Ntens),Drplde(ntens),Stran(ntens),Dstran(Ntens),
2 Predef(1), Dpred(1),Props(nprops),Coords(3),Drot(3,3),
3 Dfgrd0(3,3),Dfgrd1(3,3), time(2)

PARAMETER(ZERO=0.D0, ONE=1.D0, TWO=2.D0, THREE=3.D0,
1 FOUR=4.D0)
c..... establish limits for the stress strain behavior.
Tenlmt1 = Props(Nprops-1)
Tenlmt2 = Props(Nprops)

c
c check tension/compression
c
StrI1 = Stress (1) + Stress(2) + Stress(3)
If (StrI1 .ge. 0.01D0) then
c
c Properties for tensile behavior
c Tensile stress-strain behavior assumed to be Bi-Linear
c
If ( StrI1. Le. TenLmt1) then
c
c----- Initial Stress Strain Behavior
c
D11 = Props(1)
D12 = Props(2)
D13 = Props(3)
D22 = Props(4)
D23 = Props(5)
D33 = Props(6)
D44 = Props(7)
D55 = Props(8)
D66 = Props(9)
Else
if (StrI1 .Gt. Tenlmt1 .and. StrI1 .Le. Tenlmt2) Then
c
c----- Intermediate Stress Strain Behavior
c
D11 = Props(10)
D12 = Props(11)
D13 = Props(12)
```

```

D22 = Props(13)
D23 = Props(14)
D33 = Props(15)
D44 = Props(16)
D55 = Props(17)
D66 = Props(18)
else
c
c----- Final Stress Strain Behavior to failure
c
D11 = Props(19)
D12 = Props(20)
D13 = Props(21)
D22 = Props(22)
D23 = Props(23)
D33 = Props(24)
D44 = Props(25)
D55 = Props(26)
D66 = Props(27)
endif
End If
Else
c
c----- Stress Strain Behavior in Compression
c
D11 = Props(28)
D12 = Props(29)
D13 = Props(30)
D22 = Props(31)
D23 = Props(32)
D33 = Props(33)
D44 = Props(34)
D55 = Props(35)
D66 = Props(36)
End if
c
c Initialize Jacobian.
c
call aset (ddsdde,zero,ntens*ntens)
DDSDDE (1,1)=D11
DDSDDE (1,2)=D12
DDSDDE (1,3)=D13
DDSDDE (2,1)=D12
DDSDDE (2,2)=D22
DDSDDE (2,3)=D23
DDSDDE (3,1)=D13
DDSDDE (3,2)=D23
DDSDDE (3,3)=D33
DDSDDE (4,4)=D44
DDSDDE (5,5)=D55
DDSDDE (6,6)=D66
c
c calculate stress
c
do k1 =1, ntens
do k2 = 1, ntens

```

```
stress (k1) = stress (k1) + ddsdde (k1,k2) * dstran(k2)
end do
end do
c
return
end
```


References

1. Herbell, T.P.; and Eckel, A.J.: Ceramics for Rocket Engine Components. *Aero. Eng.*, vol. 11, no. 12, 1991, pp. 21–23.
2. Lamouroux, F.; Bourrat, X.; and Nasalain, R.: Structure/Oxidation Behavior Relationship in the Carbonaceous Constituents of 2D-C/PyC/Sic Composites. *Carbon*, vol. 31, no. 8, 1993, pp. 1273–1288.
3. Sullivan, Roy M.: A Model for the Oxidation of Carbon Silicon Carbide Composite Structures. *Carbon*, vol. 43, 2005, pp. 275–285.
4. Halbig, Michael C.: The Oxidation Kinetics of Continuous Carbon Fibers in a Cracked Ceramic Matrix Composite. NASA/TM—2001-210520, 2001. <http://gltrs.grc.nasa.gov/cgi-bin/GLTRS/browse.pl?2001/TM-2001-210520.html>
5. Ceramic Matrix Composite Design Methodology Development. Contract NAS1-01083, Southern Research Institute, Birmingham, AL, 2001.
6. Mital, S.K.; Murthy, P.L.N.; and Chamis, C.C.: Simplified Micromechanics of Plain Weave Composites. *J. Advanced Mater.*, vol. 33, no. 3, 2001, pp. 10–17.
7. Mital, Subodh K.; and Murthy, Pappu L.N.: Characterizing the Properties of a C/SiC Composite Using Micromechanics Analysis. *AIAA Paper 2001-1363*, 2001.
8. Murthy, Pappu L.N.; Mital, Subodh K.; and DiCarlo, James A.: Characterizing the Properties of a Woven SiC/SiC Composite Using W-CEMCAN Computer Code. *NASA/TM—1999-209173*, 1999.
9. MSC/ABAQUS User's Manual Version 5.6, Vols. I–III. MacNeal-Schwendler Corporation, Los Angeles, CA, 1996.
10. Materials—Silicon Carbide (SiC) Properties. <http://www.accuratus.com/silicar.html> Accessed Nov. 3, 2005.

REPORT DOCUMENTATION PAGE			<i>Form Approved OMB No. 0704-0188</i>
Public reporting burden for this collection of information is estimated to average 1 hour per response, including the time for reviewing instructions, searching existing data sources, gathering and maintaining the data needed, and completing and reviewing the collection of information. Send comments regarding this burden estimate or any other aspect of this collection of information, including suggestions for reducing this burden, to Washington Headquarters Services, Directorate for Information Operations and Reports, 1215 Jefferson Davis Highway, Suite 1204, Arlington, VA 22202-4302, and to the Office of Management and Budget, Paperwork Reduction Project (0704-0188), Washington, DC 20503.			
1. AGENCY USE ONLY (Leave blank)	2. REPORT DATE	3. REPORT TYPE AND DATES COVERED	
	March 2006	Technical Paper	
4. TITLE AND SUBTITLE		5. FUNDING NUMBERS	
Development of Design Analysis Methods for C/SiC Composite Structures		WBS-22-721-21-02	
6. AUTHOR(S)			
Roy M. Sullivan, Subodh K. Mital, Pappu L.N. Murthy, Joseph L. Palko, Jacques C. Cuneo, and John R. Koenig			
7. PERFORMING ORGANIZATION NAME(S) AND ADDRESS(ES)		8. PERFORMING ORGANIZATION REPORT NUMBER	
National Aeronautics and Space Administration John H. Glenn Research Center at Lewis Field Cleveland, Ohio 44135-3191		E-15327	
9. SPONSORING/MONITORING AGENCY NAME(S) AND ADDRESS(ES)		10. SPONSORING/MONITORING AGENCY REPORT NUMBER	
National Aeronautics and Space Administration Washington, DC 20546-0001		NASA TP-2006-214005	
11. SUPPLEMENTARY NOTES Roy M. Sullivan and Pappu L.N. Murthy, NASA Glenn Research Center; Subodh K. Mital, University of Toledo, 2801 W. Bancroft Street, Toledo, Ohio 43606; Joseph L. Palko, Connecticut Reserve Technologies, Inc., 10030 Greenwich Drive, Strongsville, Ohio 44136; and Jacques C. Cuneo and John R. Koenig, Southern Research Institute, 2000 Ninth Avenue South, P.O. Box 55305, Birmingham, Alabama 35205. Responsible person, Roy M. Sullivan, organization code RXL, 216-433-3249.			
12a. DISTRIBUTION/AVAILABILITY STATEMENT Unclassified - Unlimited Subject Category: 24 Available electronically at http://gltrs.grc.nasa.gov This publication is available from the NASA Center for AeroSpace Information, 301-621-0390.		12b. DISTRIBUTION CODE	
13. ABSTRACT (Maximum 200 words) The stress-strain behavior at room temperature and at 1100 °C (2000 °F) was measured for two carbon-fiber-reinforced silicon carbide (C/SiC) composite materials: a two-dimensional plain-weave quasi-isotropic laminate and a three-dimensional angle-interlock woven composite. Micromechanics-based material models were developed for predicting the response properties of these two materials. The micromechanics based material models were calibrated by correlating the predicted material property values with the measured values. Four-point beam bending sub-element specimens were fabricated with these two fiber architectures and four-point bending tests were performed at room temperature and at 1100 °C. Displacements and strains were measured at various locations along the beam and recorded as a function of load magnitude. The calibrated material models were used in concert with a nonlinear finite element solution to simulate the structural response of these two materials in the four-point beam bending tests. The structural response predicted by the nonlinear analysis method compares favorably with the measured response for both materials and for both test temperatures. Results show that the material models scale up fairly well from coupon to subcomponent level.			
14. SUBJECT TERMS Composite materials; User-defined material model (UMAT); Micromechanics; Four-point beam bend test; Material modeling; Sub-element testing; Composite properties		15. NUMBER OF PAGES 24	
		16. PRICE CODE	
17. SECURITY CLASSIFICATION OF REPORT Unclassified	18. SECURITY CLASSIFICATION OF THIS PAGE Unclassified	19. SECURITY CLASSIFICATION OF ABSTRACT Unclassified	20. LIMITATION OF ABSTRACT

